Analyst

PAPER

View Article Online
View Journal | View Issue

Cite this: *Analyst*, 2016, **141**, 3746

Application of fast-scan cyclic voltammetry for the *in vivo* characterization of optically evoked dopamine in the olfactory tubercle of the rat brain†

Ken T. Wakabayashi,[a,b] Michael J. Bruno,[b] Caroline E. Bass[b] and Jinwoo Park*[a,b]

Received 25th January 2016,
Accepted 1st April 2016

DOI: 10.1039/c6an00196c

www.rsc.org/analyst

The olfactory tubercle (OT), as a component of the ventral striatum, serves as an important multisensory integration center for reward-related processes in the brain. Recent studies show that dense dopaminergic innervation from the ventral tegmental area (VTA) into the OT may play an outsized role in disorders such as psychostimulant addiction and disorders of motivation, increasing recent scientific interest in this brain region. However, due to its anatomical inaccessibility, relative small size, and proximity to other dopamine-rich structures, neurochemical assessments using conventional methods cannot be readily employed. Here, we investigated dopamine (DA) regulation in the OT of urethane-anesthetized rats using *in vivo* fast-scan voltammetry (FSCV) coupled with carbon–fiber microelectrodes, following optogenetic stimulation of the VTA. The results were compared with DA regulation in the nucleus accumbens (NAc), a structure located adjacent to the OT and which also receives dense DA innervation from the VTA. FSCV coupled with optically evoked release allowed us to investigate the spatial distribution of DA in the OT and characterize OT DA dynamics (release and clearance) with subsecond temporal and micrometer spatial resolution for the first time. In this study, we demonstrated that DA transporters play an important role in regulating DA in the OT. However, the control of extracellular DA by uptake in the OT was less than in the NAc. The difference in DA transmission in the terminal fields of the OT and NAc may be involved in region-specific responses to drugs of abuse and contrasting roles in mediating reward-related behavior.

1. Introduction

The olfactory tubercle (OT) is an anatomical substructure of the ventral striatum, a brain region which additionally includes the nucleus accumbens (NAc) and the ventral pallidum (VP).[1] While the ventral striatum, as a "limbic-motor interface"[2] is thought to play a critical role in motivation and reward,[3–5] the contribution of the OT to these brain processes remains unclear. The OT acts as an integration center for multiple sensory modalities beyond that of basic odor processing,[6,7] and shares many neuroanatomical and neurochemical similarities with other ventral striatal substructures like the NAc.[8] Similar to the NAc, the OT is innervated densely by dopamine (DA) neurons originating from the ventral tegmental area (VTA).[7,9,10] VTA DA release in the NAc has been heavily implicated in reward[11–16] and as an important pathway for drugs of abuse.[17] Therefore, VTA DA in the OT may also play a role in the neural correlates of reward.[10,18–20] There is some evidence to suggest that despite similar patterns of VTA innervation, DA in the OT maybe critically involved in reward processing, potentially contributing more towards the processes underlying reward and drug addiction.[10,20,21] For these reasons, DA in the OT has begun to receive renewed attention from neuroscientists.[10]

Yet while DA is a key component of normal OT function, compared to other ventral striatal structures, DA transmission in the OT, its regulation, and functional roles are less known. This is partially due to its complicated anatomical structure, its deep ventral location proximal to the edge of the brain, and that the structure is only a few hundred microns across. These factors have limited its accessibility with other classical neurochemical monitoring techniques such as microdialysis to monitor DA solely from the OT, due to its low spatial (~hundreds μm) and temporal resolution (generally minute scale), despite advances in detection.[22] This issue is particularly highlighted in the OT due to its proximity with the NAc, another substructure heavily innervated with VTA DA neurons as described above. To overcome the lack of spatial resolution and the slow response of conventional neurochemical techniques, here we employ *in vivo* fast-scan cyclic voltam-

[a]*Department of Biotechnical and Clinical Laboratory Sciences, University at Buffalo, State University of New York, Buffalo, NY 14214, USA*
[b]*Pharmacology and Toxicology, University at Buffalo, State University of New York, Buffalo, NY 14214, USA. E-mail: jinwoopa@buffalo.edu; Fax: +1 (716) 829-3601; Tel: +1 (716) 829-5186*
†Electronic supplementary information (ESI) available. See DOI: 10.1039/c6an00196c

metry (FSCV) coupled with carbon–fiber electrodes (CFE), which can monitor local changes in DA in the OT at a subsecond timescale. FSCV is widely used for characterizing the dynamics of many electroactive neurochemicals including norepinephrine, serotonin, hydrogen peroxide and oxygen in the brain.[23–25] The background-subtracted cyclic voltammograms of electroactive compounds provide "electrochemical fingerprints" based on their oxidation and reduction potentials. Thus in contrast to other electrochemical approaches such as amperometry, which only provides quantitative information (*i.e.* changes in concentration), FCSV provides both quantitative and qualitative (*i.e.* identification) information of neurochemicals from other interferences such as their metabolites and ascorbic acid, often present in the brain near the CFE.[23] Therefore, this approach with high temporal and spatial resolution enabled us to characterize the dynamics of extracellular DA in the OT.

Optogenetics is a technique where light can be used to activate a light-sensitive ion channel (*e.g.* channelrhodopsin-2, ChR2) which causes the neuron to fire.[15,26–29] By introducing ChR2 into a specific brain region, most often with a viral vector, the resulting ChR2 expression can be restricted to a specific brain region, and either the cell bodies or their terminals can be stimulated directly. In this study, we have used an adeno-associated virus (AAV) to deliver the ChR2 gene to the VTA. AAV has numerous properties that make it an ideal delivery vehicle in neurochemical studies. For example, AAV primarily infects neurons, does not elicit an immune response, and is extremely long-lasting, even though the viral DNA is primarily episomal (*i.e.* it does not integrate into the host genome). The AAV used in this study delivers a ChR2-EYFP transgene driven by a generalized non-restricted promoter. While this promoter is ubiquitous, the AAV serotype we used (AAV10) transduces primarily neuronal cell bodies, and will not infect fibers of passage or terminals within the VTA.[30,31] This is a key advantage of this approach, as the noradrenergic bundle containing axons of noradrenergic cell bodies passes near the VTA.[32,33] While electrical stimulation of the VTA also stimulates this noradrenergic pathway and evokes norepinephrine release[34,35] in caudal portions of the NAc,[36] optical stimulation should eliminate the contribution of this potential confound in the OT. It is also noteworthy that while cyclic voltammograms provide an electrochemical "fingerprint" that can be used to identify catecholamines from other substances such as their metabolites and ascorbic acid, FSCV cannot distinguish between DA and norepinephrine due to their similar electrochemical properties.

By incorporating these two techniques, the objective of this study is to show for the first time how optically evoked DA is regulated in the small OT (~500 μm across) with FSCV. Here, we compare the dynamics, relative concentrations, and effects of selective DA drugs on DA release and clearance in the OT to that of the NAc, a neighboring ventral striatal structure. Moreover, our results here show that FSCV can be successfully employed along with optogenetic control of DA release to monitor relatively inaccessible substructures of the ventral striatum.

2. Experimental

Adeno-associated virus (AAV) packaging

The EF1α-ChR2-EYFP AAV plasmid was a kind gift from K. Deisseroth and contains AAV2 terminal repeats flanking a transgene cassette consisting of the EF1α promotor followed by a ChR2-EYFP fusion gene, woodchuck post-regulatory element (WPRE), and a human growth hormone polyA sequence. Packaging of the EF1α-ChR2-EYFP-AAV plasmid was conducted as described previously.[29] Briefly, a standard triple transfection protocol was used to create helper virus-free pseudotyped AAV2/10 virus.[37] An AAV2/10 rep/cap plasmid provided the AAV2 replicase and AAV10 capsid genes,[38] while adenoviral helper functions were supplied by pHelper (Stratagene, La Jolla). AAV-293 cells (Strategene, La Jolla, CA) were transfected with 10 μg of pHelper, and 1.15 pmol each of AAV2/10 and AAV vector plasmids *via* calcium phosphate precipitation. The cells were harvested 72 hours later and the pellets resuspended in DMEM, freeze–thawed three times, and centrifuged multiple times to produce a clarified viral lysate.

Stereotaxic virus injection

Male Sprague-Dawley rats (300–350 g; Wilmington, MA, USA) were anesthetized with ketamine hydrochloride (75 mg kg^{-1} i.p.) and xylazine hydrochloride (10 mg kg^{-1}, i.p.) and placed in a stereotaxic frame (David Kopf Instruments). The scalp was chemically depilated, and swabbed with iodine and ethanol. Pre-incision local anesthesia was induced by an injection of bupivacaine (1.6 mg kg^{-1} s.c.), and a central incision was made to expose the skull. A small hole (~0.5 mm in diameter) was drilled above the right VTA (from bregma: anteroposterior (AP), −5.2 mm; mediolateral (ML), +1.0 mm) according to the coordinates of Paxinos and Watson.[39] Then, a Hamilton syringe containing 1.5 μl virus was lowered into the VTA (dorsoventral (DV), −7.8 mm). The virus was injected at a rate of 0.5 μl min^{-1}, and the syringe was allowed to remain in place for 4 minutes after the injection to limit diffusion before it was slowly retracted. The scalp was then sutured, and rats were returned to their home cages after recovery from anesthetic. All protocols were approved by the Institutional Care and Use Committee at the University at Buffalo. All experiments complied with the "Guide for the Care and Use of Laboratory Animals" (8th edition, 2011, US National Research Council).

Fast-scan cyclic voltammetry

Over 30–40 days after the virus injection, rats were anesthetized with urethane (1.5 g kg^{-1}, i.p.) and placed in a stereotaxic frame. The dorsal skull surface was exposed, and the hole used to inject the virus above the VTA was carefully re-drilled and cleaned. Additional small holes were drilled in the skull for the carbon–fiber microelectrode (from bregma: AP + 1.8 mm, ML −1.0 mm, DV −6.0 mm–8.5 mm) and the reference electrode (Ag/AgCl, contralateral hemisphere). Glass-encased cylindrical carbon–fiber microelectrodes consisting of untreated T-650 untreated fibers (Cytec Industries Inc., Greensville, SC, USA) with an exposed length of 80–100 μm and 7 μm

nominal diameter were constructed and used as previously described.[40] A scanning electron micrograph of an example CFE is shown in ESI Fig. S1.† Extracellular DA was monitored at the carbon–fiber microelectrode every 100 ms with a triangular waveform (−0.4 to +1.3 V, 400 V s^{-1}). The triangular waveform was low-pass filtered at 2 kHz. Data were digitized and processed using NI-6711 and NI-6251 DAQ/ADC cards (National Instruments, Austin, TX, USA) and TH-1 software. Digitized data were stored on a computer. Voltammetric responses were viewed as color plots with the abscissa as voltage, the ordinate as acquisition time, and the current encoded as color.[41] Cyclic voltammograms during optical stimulation were background subtracted digitally from those collected during baseline recording. The oxidation current was converted to concentration based on the averaged DA calibration factor of 9.2 pA ± 1.1 (μM μm^2). The DA calibration factor was determined *in vitro*, in a Tris buffer solution at pH 7.4 containing 15 mM Tris, 140 mM NaCl, 3.25 mM KCl, 1.2 mM $CaCl_2$, 1.25 mM NaH_2PO_4, 1.2 mM $MgCl_2$, and 2.0 mM Na_2SO_4 in double-distilled water.

Optical stimulation

Optical stimulation was achieved by a 473 nm laser (Viasho, Beijing, China) with a maximum output of 100 mW. The laser was fiber pigtailed into a glass fiber with a 200 μm diameter core (Thorlabs, Newton, New Jersey, USA), and delivered into the brain *via* an optical cannula consisting of a bare optical fiber and fiber ferrule (O.D. 240 μM, I.D. 200 μM, Doric Lenses, Canada) implanted in the VTA (DV: 7.7 mm–9.0 mm). The laser was modulated using a USB-TTL interface (Prizmatics, Israel), controlled by a desktop computer which allowed for the control of the frequency of the square pulses (between 1–80 Hz), the total number of pulses (between 1–120) in one data stream, and the width of each pulse as a fraction of the period between the pulses (between 1–9 ms). Two separate computers were used to control both the voltammetric recordings and an acquisition unit used to control the laser, and were manually synchronized by the experimenter.

Histological verification

At the end of the recording, the carbon–fiber microelectrode placement was verified by applying a constant current (max 20 μA for 10 s) directly to the electrode.[34–36] Rats were then euthanized with an overdose of urethane and transcardially perfused with phosphate buffered saline (PBS, 23 °C) followed by 10% formalin. Brains were stored in formalin for 24 hours at 4 °C and then transferred to 30% sucrose for a minimum of 3 days. They were then sectioned at 50 μm on a sliding microtome. Freely floating coronal sections were quickly screened by visualizing the attached EYFP fluorescent tag which was co-expressed with ChR2 using a fluorescent stereomicroscope (Kramer Scientific, MA, USA) that had been modified to accept a liquid light guide attached to an EXPO X-Cite 120 fluorescent illumination source. Images were acquired with a Lumenera Infinity 3-1 Monochrome Camera (Ottawa, Canada) and the 8-bit grayscale images were pseudocolored using the Fire-Look Up Table (LUT) in ImageJ. Carbon–fiber microelectrode and optrode placements were confirmed at the same time using episcopic white light illumination.

Data and statistical analysis

Data were analyzed in GraphPad Prism (GraphPad Software version 6.0, San Diego, CA, USA). A Student's *t*-test, and two-way ANOVAs were used to determine statistical significance. '*n*' values indicate the number of rats. The data are presented as mean ± SEM, and the criterion of significance was set at $p < 0.05$.

Drugs and reagents

All chemicals and drugs were reagent-quality and were used without additional purification. Drugs were obtained from Sigma-Aldrich (St. Louis, MO, USA). Raclopride-HCl, was dissolved in sterile saline. GBR-12909-HCl was dissolved in double-distilled water and then further diluted with sterile saline. All drugs were injected intraperitoneally.

3. Results and discussion

Optically evoked DA release in the OT is spatially distinct from the NAc

The OT comprises a relatively small region (~500 μm across in the dorsoventral plane) of the ventral striatum, where the anteromedial portion is ventral to the NAc.[1,7] Thus, light evoked DA release in the ventral striatum was recorded by lowering carbon–fiber microelectrodes through the NAc (6.0 mm–8.0 mm from the skull surface) to the OT (8.0 mm–8.5 mm) while the optrode was fixed in the VTA ~8.5 mm from the skull surface. Fig. 1A shows a schematic representation of the path of the microelectrode (track shown by a dotted line) used for DA measurements in the NAc and OT. We chose these locations based on previous studies suggesting that the functional role of DA in the NAc and the anteromedial compartment of the OT may differ with reward-related behavior.[7,10] The microelectrode was lowered in the NAc and OT at 0.2 and 0.1 mm increments, respectively, and optical stimulation (40 Hz, 60 pulses) was delivered at different depths at 4–5 min intervals. Fig. 1D shows a representative temporal DA concentration trace at different depths. As the microelectrode transited through the NAc, optically evoked DA release was observed ~6.0 mm and the maximal release was seen between 6.6 mm and 7.0 mm. As the electrode advanced, evoked DA release decreased, reaching a relative nadir ~7.7 mm below the skull surface, which is consistent with previous studies showing electrically evoked DA release in the NAc.[36] The optically evoked signal increased again between 8.0 mm and 8.4 mm, corresponded to the depth of the OT. The cyclic voltammograms recorded at the depth of maximal release in the NAc and OT showed the characteristic oxidation current of DA observed at ~+0.6 V, and the peak for the reduction of the electrically formed DA-*o*-quinone at ~−0.2 V on the reverse scan (Insets of Fig. 1D). Lowering the electrode further caused it to

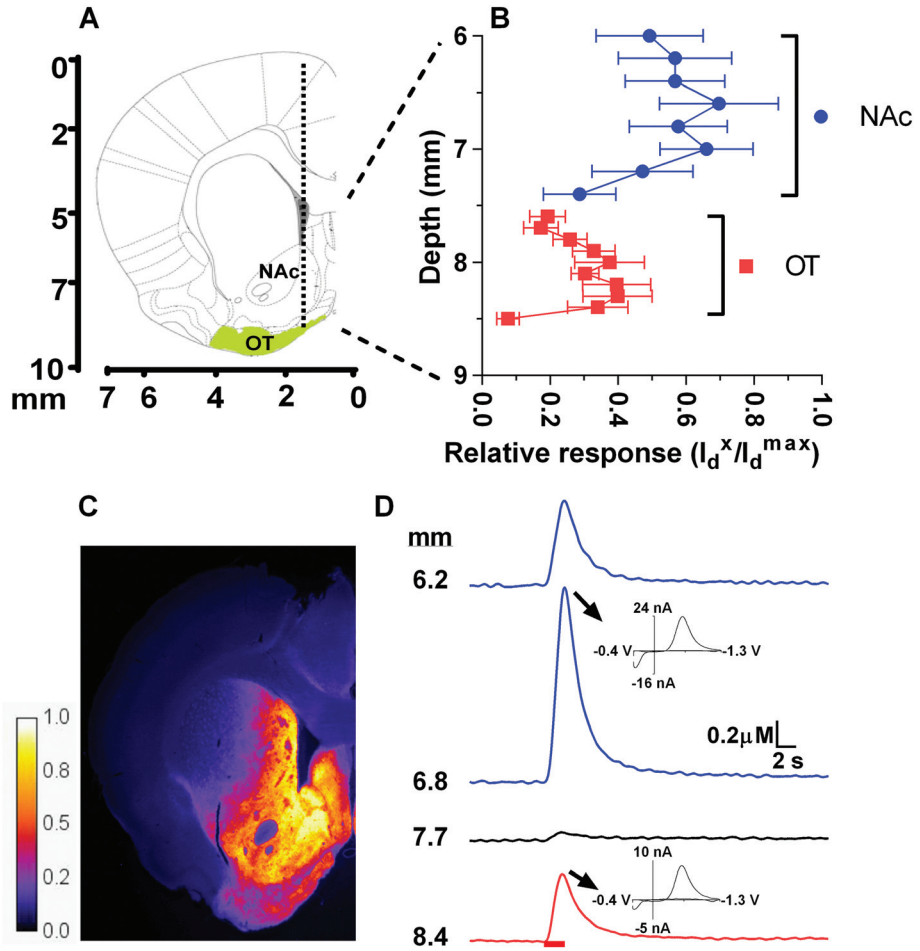

Fig. 1 Map of optically evoked DA responses in the NAc and OT as a function of the depth of the microelectrode. A is a coronal section (AP + 1.8 mm from bregma, from Paxinos and Watson[39]) schematically showing the approximate path of the microelectrode aimed at the NAc and OT (filled color). B shows the relative response of DA in the NAc and OT evoked by optical stimulation (40 Hz, 60 pulses, 4 ms) at different depths of the carbon–fiber microelectrode, (I_d^x/I_d^{max}), where I_d^x is the response at a particular depth divided by the maximal response, I_d^{max} of DA in the NAc evoked at different positions of the carbon–fiber microelectrode (n = 4). C shows a representative 50 μm thick section showing ChR2 expression in the terminal fields of the OT and the NAc as the native florescence of the ChR2-EYFP fusion protein. Images were pseudocolored to enhance contrast, and the scale indicates relative intensity of the EYFP signal. D shows representative DA concentration *versus* time traces for DA at different depths of the working electrode in the same animal, insets show the distinct cyclic voltammogram for DA at the peak concentration values. Red bar denotes stimulation interval.

break against the ventral skull within 0.2–0.3 mm. Evoked DA release in the OT was observed over a much narrower distance than in the NAc, along with a sharp drop in evoked release near the ventral border of the brain corresponding to the anatomical characteristics of the OT. Each individual recording evidenced this spatial pattern, seen in the average relative response (Fig. 1B), clearly delineating two spatially distinct areas. The second increase in evoked DA release in the OT was 57.2 ± 0.15 percent of the relative evoked release observed in the NAc. An individual example of the microelectrode location in the OT visualized by a post-experiment lesion is shown in ESI Fig. S2.† Expression of ChR2 was observed in the terminal regions of the NAc and OT after the incubation period, as seen in the representative example (Fig. 1C). It should be noted that ChR2 expression and optically evoked DA release depends in part on where the virus was injected and where the optrode was placed, respectively. In some brains, ChR2 expression was observed in the dorsal striatum as well, depending on the localization of the VTA virus injection, and a result of the dispersion of the virus.

DA release in the OT is dependent on stimulating optrode depth and is restricted to areas of ChR2 expression

To determine the optimal stimulation depth of the VTA, optically evoked DA responses (40 Hz, 60 pulses) were measured while the working microelectrode was fixed in position in the OT. Fig. 2A shows a schematic representation of the path of the optrode in the VTA (dashed line). The stimulating optrode was lowered from 7.0 mm to 9.2 mm relative to the skull with ~0.2 mm increments. When averaged across multiple animals, the relative intensity of the optically evoked DA signal was not observed above 7.6 mm and began to be monitored at

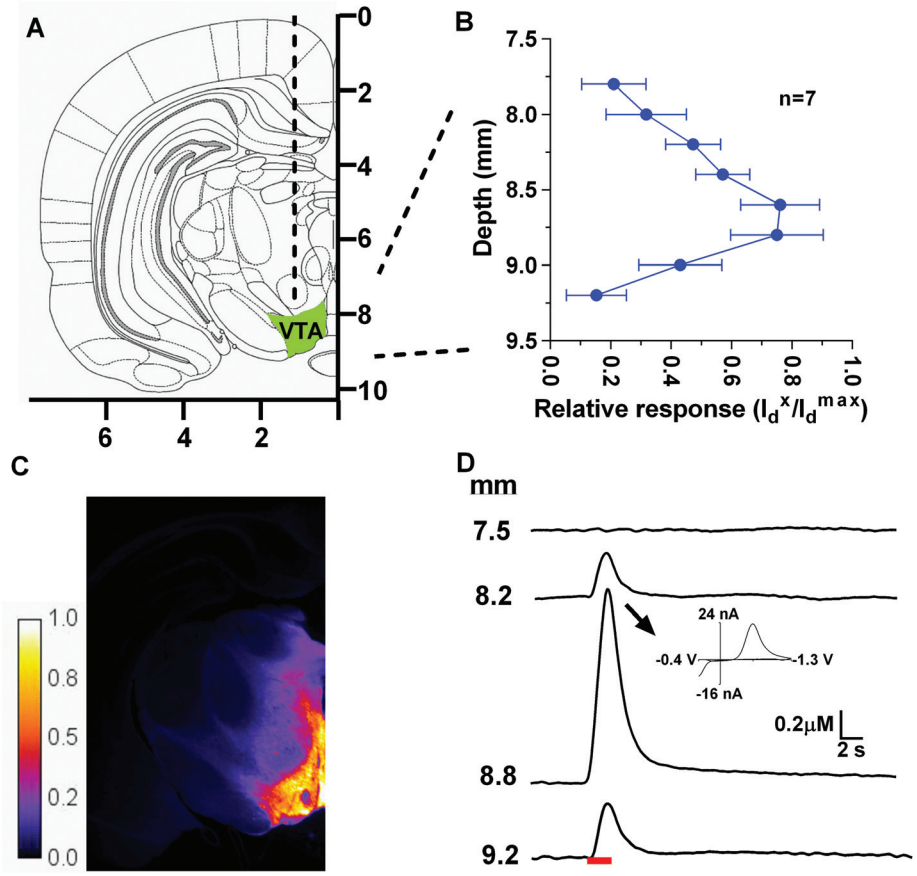

Fig. 2 Map of optically evoked DA responses in the OT as a function of the depth of the stimulating optrode. A is a coronal section (AP −5.3 mm from bregma, from Paxinos and Watson[39]) schematically showing the approximate path of the stimulating optrode aimed at the VTA (filled color). B shows the relative response (I_d^x/I_d^{max}), where I_d^x is the response at a particular depth divided by the maximal response, I_d^{max} of DA in the OT evoked at different positions of the stimulating optrode. C shows a representative 50 μm section showing Ch2R expression in the VTA as the native florescence of the ChR2-EYFP fusion protein. Images were pseudocolored to enhance contrast, and the scale indicates relative intensity of the EYFP signal. D shows representative evoked DA concentrations in the OT *versus* time traces for DA at different depths of the optrode (40 Hz, 60 pulses, 4 ms) in the same animal. The inset shows the distinct cyclic voltammogram for DA at the peak concentration value. Red bar indicates stimulation interval.

~7.8 mm at the depth where the virus was infused into the VTA (Fig. 2B). Maximal optically evoked release in the OT was seen between 8.6 mm and 8.8 mm from the skull surface. Individual DA concentration traces recorded in the OT are shown in Fig. 2D. Robust expression of ChR2 was also observed in the VTA, with peak expression restricted to the VTA (Fig. 2C). An individual example of an optrode placement in the VTA is shown in ESI Fig. S3.† It is well known that bipolar stimulating electrodes (composed of two stainless-steel electrodes, each electrode O.D. 0.2 mm) used to activate the VTA electrically, cause tissue damage. The histology shows that the optrode (O.D. 0.24 mm) also has an impact on the tissue but the single probe of the optrode causes less tissue damage than the bipolar stimulating electrodes, while offering better spatial resolution.

Monitoring different DA dynamics in the OT and NAc

Optical stimulation (40 Hz, 60 pulses, 4 ms) to the VTA expressing ChR2 induces DA release in the OT and NAc in a single animal (Fig. 3). Both voltammograms in the OT (Fig. 3A) and NAc (Fig. 3B) are due to DA, as catecholamines like DA are oxidized to its *ortho*-quinone form at ~+0.6 V and the reduced back to DA at ~−0.2 V as described above. Although norepinephrine can also exhibit similar electrochemical characteristics as DA, its contribution to the observed signal should be minimal because optical stimulation to the VTA should only stimulate neuronal cell bodies and not stimulate noradrenergic fibers of passage near the VTA. Additionally, at this anatomical coordinate, evoked NE release in the NAc and OT is negligible based on previous electrochemical[36] and HPLC[42,43] data. The current at ~0.6 V in both regions rapidly increased during optical stimulation, and afterwards decreased back to pre-stimulation levels.

The average maximal DA concentration ($[DA]_{max}$) evoked by optical stimulation at 40 Hz in the OT was ~1.7 fold less than the $[DA]_{max}$ in the NAc[34,36] (Table 1). However, the half-decay time ($t_{1/2}$), the time needed for DA to descend from its maximum to half of its value, were significantly longer in the OT than in the NAc ($p < 0.05$, Table 1), indicating slower clearance of evoked DA in the OT. The lower $[DA]_{max}$ and its slower disappearance in the OT may be due to less dense DA term-

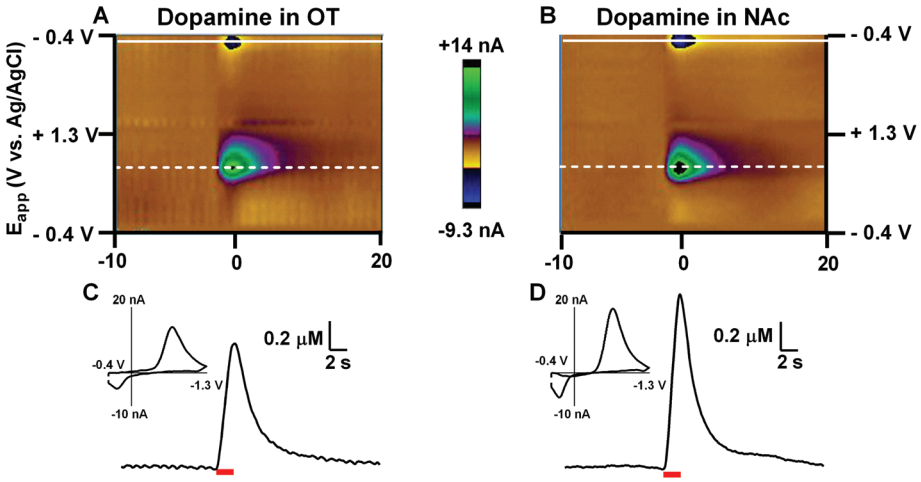

Fig. 3 Representative optically evoked DA signals recorded in the OT (A) and NAc (B). Upper panels are color plots for the voltammetric data shown for each example, with current changes encoded in false color. The red bars under the current traces indicate the stimulation interval (40 Hz, 60 pulses, 4 ms). The sets comprised of all background-subtracted cyclic voltammograms recorded for 10 s before and 20 seconds after optical stimulation. DA concentration changes are apparent at the potential for its oxidation (~+0.6 V, dotted line) and reduction (~−0.2 V, solid line). Changes in concentrations for each stimulation are shown at the maximum of evoked release. Background-subtracted cyclic voltammograms are shown as insets at the maximum of evoked release.

Table 1 Numerical parameters measured from optically evoked DA in the OT and NAc evoked by optical stimulation (40 Hz, 60 pulses)

Rats (n = 7)	DA in the OT	DA in the NAc
$[DA]_{max}$ (μM)	0.34 ± 0.24	0.59 ± 0.01
$t_{1/2}$ (s)	3.05 ± 1.12*	1.14 ± 0.12

$[DA]_{max}$ is the maximal optically evoked DA concentration, $t_{1/2}$ is the time required for DA overflow to decay to 50% of the maximum. Values represent the mean ± SEM. Values were compared by unpaired t-tests. * indicates a significant difference between OT and NAc (t_8 = 2.76, $p < 0.05$).

inals and DA transporter (DAT) expression compared to NAc.[44–46] Consequently, the rate of extracellular DA removal in the OT may be less, which functionally may allow DA more time to diffuse away from its release site than in the NAc, allowing volume transmission. Compared to the range reported for electrically evoked $[DA]_{max}$ in the NAc, light evoked $[DA]_{max}$ in the NAc was lower and more variable (Table 1).[34,36] Likely, this was a result of variation in ChR2 expression in the stimulating area, differences in the area of effect, along with differences in the intensity between light and electrical stimulation, and that optical stimulation restricts its effect to neurons expressing ChR2, and does not affect non-expressing neurons and fibers passing through the VTA.

DA responses in the NAc and OT to various optical stimulation parameters

Optically evoked DA release depends on different stimulation parameters (frequency, pulse number, and pulse duration) and optimum parameters are not well established and will differ lab to lab. Thus, we investigated DA responses in the OT and NAc to different optical stimulation parameters to find the optimum conditions in order to achieve reproducible signals and to mimic natural phasic DA release in the brain (Fig. 4). There was an overall effect of changing the stimulus frequency on evoked DA release in both the OT (Fig. 4A) and NAc (Fig. 4D) assessed by a Two-Way Repeated Measures (RM) ANOVA (Fig. 4F, main effect of frequency $F_{5,\ 40}$ = 3.44, $p < 0.05$), but there were no other significant differences. Increasing the frequency of optical stimulation between 5–40 Hz (4 ms pulse width, 60 pulses) resulted in an increase in relative evoked DA release in both the OT and the NAc. Optical stimulation resulting in DA release generally showed two types of frequency dependent dynamics in both the NAc and OT – steady state release at lower stimulation frequencies (<20 Hz), and peak-shaped evoked signals at higher frequencies (≥20 Hz). The characteristics of DA signals at different frequencies depend on the rapidity of stimulation, and on the rate of DA clearance and release.[47–49] At lower frequencies, sufficient time exists for the release and uptake of DA to equalize, while the shorter time between stimulus pulses at higher frequencies permits release to overtake clearance, resulting in peak-shaped signals largely dependent on the magnitude of DA release in both OT and NAc. At higher frequencies greater than 40 Hz, the relative DA response decreased. This inverted U-shaped frequency dependence has been previously shown following ChR2 mediated optically evoked DA release in the nigrostriatal pathway.[29] As in the dorsal striatum, this frequency response in the OT and NAc may reflect the photocycle kinetic properties of the Ch2R protein[26,50] and potassium and sodium channel kinetics in the host neuron,[51] resulting in DA neurons unable to respond to higher frequencies of optical stimulation.

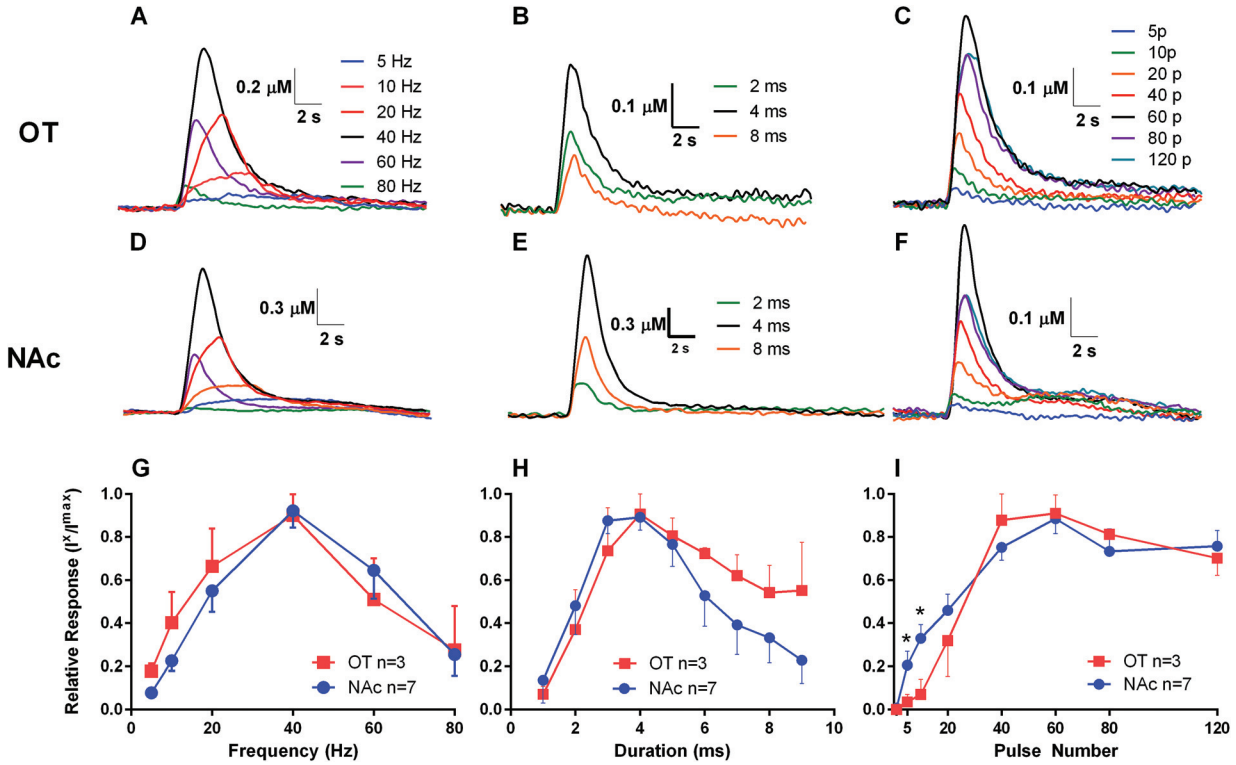

Fig. 4 Comparison of representative DA responses in the OT and NAc as a function of frequency (A, D), pulse duration (B, E) and pulse number (C, F). Maximal mean [DA] responses in the NAc and OT as a function of frequency (G), pulse duration (H), and pulse number (I) shown as relative response (monitored DA response (I^x)/maximal response (I^{max})). * Significantly different response between the OT and NAc during evoked [DA].

Increasing the pulse duration from 1–4 ms (40 Hz, 60 pulses) also resulted in a similar increase in subsecond DA release in both the OT (Fig. 4B) and NAc (Fig. 4E) where there was a significant effect of duration (Fig. 4G, main effect of duration, $F_{8,\ 64} = 6.82$, $p < 0.05$), but no other significant differences. Relative maximal release occurred at 4 ms. Increasing the pulse duration further resulted in a decrease in evoked DA release in both regions. This finding is in agreement with previously published reports with optically evoked nigrostriatal DA release, where shorter duration pulses better mimicking physiological conditions were able to evoke greater DA release than longer pulse durations in an intact brain.[29]

Altering the pulse number from 1–120 pulses (40 Hz, 4 ms) resulted in an increase in optically evoked DA release in both the OT (Fig. 4C) and NAc (Fig. 4F) (Main effect of pulse number $F_{7,\ 56} = 34.6$, $p < 0.05$, Fig. 4I) up to 60 pulses per stimulation, similar to published reports using the same virus to stimulate nigrostriatal DA release.[52] At these lower pulse numbers, the NAc appeared to be slightly more sensitive to increases in pulse number than the OT. Thereafter, increasing pulse number over 60 pulses resulted in no significant increases in either the OT or NAc. One explanation is that DA in both substructures is highly regulated with greater presynaptic inhibition by D2 autoreceptors, leading to a greater control of release with longer periods of stimulation. Alternatively, this parameter may also be limited by ChR2 protein kinetics at higher pulse numbers.[29]

Selective DA drugs impact stimulated DA release differently in the OT and in the NAc

To further assess the regulation of DA in the OT, we characterized the effects of a selective DAT and a D2-autoreceptor inhibitor on optically evoked release. Both presynaptic D2 autoreceptors and the DAT play key roles in modulating DA release and removal, respectively, in the ventral striatum. However, not much is known about how DA release in the OT is regulated by DAT and its presynaptic D2-receptors. Therefore, in the next experiment, we assessed the impact of systemically administering the D2 antagonist, raclopride (RAC), and the selective DAT uptake blocker, GBR-12909 (GBR), on optically evoked DA in the OT, and determined how evoked DA dynamics are modulated by the drugs and compared to the result from the NAc. Before intraperitoneal (i.p.) drug administration, optically evoked DA in the OT at 20 Hz with 60 pulses were recorded every 5 min for ~30 min as a control (OT: $[DA]_{max}$ = 0.21 ± 0.16 μM, NAc: $[DA]_{max}$ = 0.24 ± 0.08 μM) as described in previous studies.[36] We chose 20 Hz because lower frequency evoked release and clearance are more effectively modulated by D2 autoreceptors and DAT, respectively,[53] resulting in a more significant effect of the DA drugs on extracellular DA concentration.

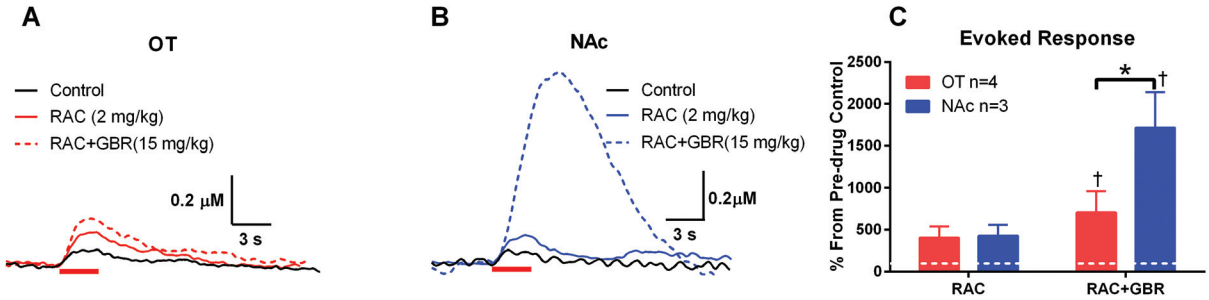

Fig. 5 Effect of selective DA pharmacological agents raclopride, (RAC, 2 mg kg^{-1}, i.p.), GBR-12909 (GBR, 15 mg kg^{-1}, i.p.) on optically evoked release (20 Hz, 60 pulses) and uptake in the OT and NAc. RAC increased $[DA]_{max}$ and $t_{1/2}$ in the representative examples of evoked release in the OT (A, solid red line) and NAc (B, solid blue line). Subsequent GBR administration further increased both [DA] and $t_{1/2}$ in both structures (OT: dashed red line, NAc: dashed blue line). These effects were reflected in the group means (C), where a 2-way RM ANOVA revealed a main effect of drug ($F_{2,\ 10}$ = 16.4, $p < 0.05$) and a significant drug × region interaction ($F_{2,\ 10}$ = 4.35, $p < 0.05$). One-sample *t*-tests revealed significant differences between controls (white dashed line) and RAC + GBR in the OT and NAc (†, OT: t_3 = 2.38, NAc, t_2 = 3.81, $p < 0.05$). A planned comparison between the effects of RAC + GBR revealed a significant difference in the OT and NAc (t_5 = 2.18, $p < 0.05$).

Twenty minutes after the administration of the D2 antagonist, RAC (2 mg kg^{-1}, i.p.), optically evoked DA (Fig. 5) and its $t_{1/2}$ value significantly increased in both the OT and NAc to similar levels compared to control values (Fig. 5A). Subsequent administration of the DAT inhibitor GBR (15 mg kg^{-1}, i.p.) further increased evoked DA concentrations in the OT and NAc and reached its maximum, 50–60 minutes after administration. These pharmacological studies reveal that D2 autoreceptors and DAT in both regions play a key role in regulating extracellular DA levels. The average results from all animals show that there was an overall effect of drugs in both the OT and NAc on evoked DA concentrations (main effect of drug $F_{2,\ 10}$ = 16.8, $p < 0.05$), and the effect of drugs differed between each region (region × drug interaction $F_{2,\ 10}$ = 4.3, $p < 0.05$). While RAC increased both evoked concentration and $t_{1/2}$, and these increases were further enhanced significantly by GBR in both regions, GBR with RAC on board had a lesser effect on evoked DA concentration in the OT than in the NAc (Fig. 5 and Table 2). Given that the control $t_{1/2}$ of DA in the OT was longer than that in the NAc (Table 2), together this may indicate that DA is less regulated in the OT by DAT than in the NAc. This finding is in agreement with other studies that have found less DAT expression in the OT using autoradiography.[54] This may have important functional implications, as a slower clearance rate in the OT could lead to the persistence of DA in the extracellular space, and allowing DA to impact a greater number of neurons through diffusion and extrasynaptic volume transmission. Moreover, many commonly abused psychostimulants such as amphetamine and cocaine interact with the DAT as one of their mechanisms of action.[55–57] Less DAT expression may help explain why locally microinjected drugs have a greater behavioral effect in the OT than the NAc.[10] It should be noted however, that the systemic administration of RAC and GBR does not limit their actions solely to the terminal regions of the OT and NAc. Other parts of the brain could also be affected, indirectly impacting evoked release in either the NAc or OT.

Table 2 Effect of the D2 antagonist raclopride (RAC, 2 mg kg^{-1}) and DAT uptake inhibitor GBR-12909 (GBR, 15 mg kg^{-1}) on optically evoked DA clearance ($t_{1/2}$) in the NAc and OT

Drug	% of Control half-decay time ($t_{1/2}$) at 20 Hz	
	DA in OT	DA in NAc
Control	$t_{1/2}$ = 2.19 ± 0.72 s†	$t_{1/2}$ = 1.07 ± 0.29 s
RAC	189 ± 19*	290 ± 76
RAC + GBR	352 ± 26*†	508 ± 74*

Data are mean ± SEM and were obtained during 20 Hz stimulations (60 pulses). Pre-drug control values ($t_{1/2}$, the time required for DA overflow to decay to 50% of the maximum) are shown as numerical values. Effects of the DA drugs on $t_{1/2}$ are shown as percent change from pre-drug control. * Significantly different from control values. † Significant difference between the NAc and OT.

DA transients in the OT following combined inhibition of DA uptake and D2-autoreceptors

Naturally occurring DA transients are observed in awake rats[58] as a result of burst firing of DA neurons in the VTA.[59] In contrast, in deeply anesthetized rats these DA transients are rarely seen,[60] except under D2 receptor antagonism and DAT blockade. This combination of drugs leads to increased burst firing and slow rhythmic oscillations in the firing rate of VTA DA neurons in anesthetized rats.[61] Therefore, while naturally occurring spontaneous DA transients are significantly reduced by anesthesia due to the reduction of dopaminergic neuron firing, co-administration of D2 receptor antagonists and DAT inhibitors can enhance extracellular DA concentration changes so that it can be measured.[34] It has been previously shown that these spontaneous phasic DA transients can be observed in the dorsal striatum[60] and the NAc.[34,36] Thus, we assessed whether the OT exhibits similar patterns of DA transients after administration of both drugs. Spontaneous DA transients were clearly observed in the OT after the administration of the two DA drugs (Fig. 6). The responses were considered significant if their magnitudes were larger than 3 times the standard deviation of the noise (S/N ≥ 3). The average amplitude of these transients in the OT was 0.09 ± 0.01 μM after drug administration, which was lower than those reported in the NAc in previous studies.[36]

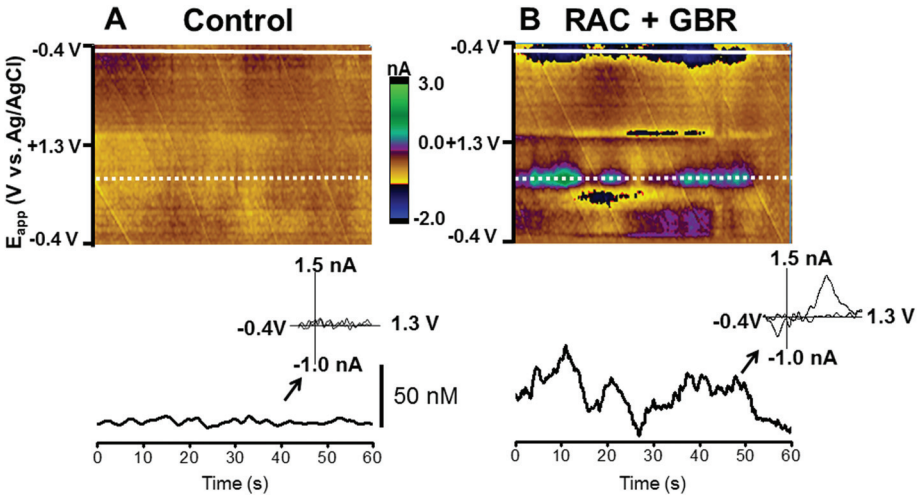

Fig. 6 Combined inhibition of DA uptake and D2 blockade induces spontaneous DA transients in the OT. Two-dimensional color plots representations of background subtracted cyclic voltammograms collected over 60 s before A and after B raclopride (RAC, 2 mg kg^{-1}, i.p.) and GBR-12909 (GBR, 15 mg kg^{-1}, i.p.) administration. DA concentration changes are seen in the color plot at the potential for DA oxidation (~0.6 V, dashed white line) and its reduction (~−0.2 V, solid white line). The time course of the DA concentration transients are shown below each color plot in A and B. Cyclic voltammograms are shown as insets recorded at the time indicted by the arrows were identical to that for DA in B.

4. Conclusions

In vivo FSCV with microelectrodes coupled with optogenetic control over DA release was employed for the first time to provide new insights into DA regulation in the OT, a subterritory of the ventral striatum that has not been extensively explored. The small size of the microelectrode allowed us to spatially distinguish DA regulation in the OT from that of the NAc, an adjacent structure, which cannot be achieved using other *in vivo* neurochemical methods. A comparison of DA transmission in the terminal fields of the OT and the adjacent NAc revealed subtle but key differences in the regulation of extracellular DA through DAT, despite sharing similar mesolimbic inputs. A better understanding of DA regulation in these structures may be important from a therapeutic perspective, as recent studies using positron emission tomography (PET) in cocaine abusers exhibit an altered ventral striatal and thalamic DA response to an acute stimulant challenge.[62,63] As PET has a low spatial resolution, this leaves open the possibility that subregions of the ventral striatum and the OT, which in humans is adjacent to the thalamus, respond differently to stimulants after extensive drug experience *via* alterations in terminal field DA regulation. This may help explain region-specific responses to drugs of abuse, and may highlight distinct functional roles for these different brain regions in reward-related behavior and the transition to addiction.

Acknowledgements

This work is supported by the SUNY Brain Network of Excellence Post-doctoral Fellow program (K.T.W.) and a start-up fund from the University at Buffalo-SUNY. We thank Rohan V. Bhimani for helpful comments regarding an early draft of the manuscript, and Peter Bush for assistance in SEM imaging.

References

1 S. Ikemoto, *Neurosci. Biobehav. Rev.*, 2010, **35**, 129–150.
2 G. J. Mogenson, D. L. Jones and C. Y. Yim, *Prog. Neurobiol.*, 1980, **14**, 69–97.
3 R. N. Cardinal, J. A. Parkinson, J. Hall and B. J. Everitt, *Neurosci. Biobehav. Rev.*, 2002, **26**, 321–352.
4 A. E. Kelley, *Neurosci. Biobehav. Rev.*, 2004, **27**, 765–776.
5 S. N. Haber, in *Neurobiology of Sensation and Reward*, ed. J. A. Gottfried, Boca Raton, FL, 2011.
6 D. W. Wesson and D. A. Wilson, *Neurosci. Biobehav. Rev.*, 2011, **35**, 655–668.
7 S. Ikemoto, *Brain Res. Rev.*, 2007, **56**, 27–78.
8 G. F. Alheid and L. Heimer, *Neuroscience*, 1988, **27**, 1–39.
9 P. Voorn, B. Jorritsma-Byham, C. Van Dijk and R. M. Buijs, *J. Comp. Neurol.*, 1986, **251**, 84–99.
10 S. Ikemoto, *J. Neurosci.*, 2003, **23**, 9305–9311.
11 G. D. Stuber, M. F. Roitman, P. E. Phillips, R. M. Carelli and R. M. Wightman, *Neuropsychopharmacology*, 2005, **30**, 853–863.
12 J. J. Day and R. M. Carelli, *Neuroscientist*, 2007, **13**, 148–159.
13 P. E. Phillips, G. D. Stuber, M. L. Heien, R. M. Wightman and R. M. Carelli, *Nature*, 2003, **422**, 614–618.
14 I. A. Yun, K. T. Wakabayashi, H. L. Fields and S. M. Nicola, *J. Neurosci.*, 2004, **24**, 2923–2933.
15 H. C. Tsai, F. Zhang, A. Adamantidis, G. D. Stuber, A. Bonci, L. de Lecea and K. Deisseroth, *Science*, 2009, **324**, 1080–1084.

16 M. J. Wanat, I. Willuhn, J. J. Clark and P. E. Phillips, *Curr. Drug Abuse Rev.*, 2009, **2**, 195–213.
17 R. A. Wise, *Nat. Rev. Neurosci.*, 2004, **5**, 483–494.
18 R. Prado-Alcala and R. A. Wise, *Brain Res.*, 1984, **297**, 265–273.
19 M. A. Gadziola and D. W. Wesson, *J. Neurosci.*, 2016, **36**, 548–560.
20 B. M. Striano, D. J. Barker, A. P. Pawlak, D. H. Root, A. T. Fabbricatore, K. R. Coffey, J. P. Stamos and M. O. West, *Synapse*, 2014, **68**, 321–323.
21 L. H. Sellings, L. E. McQuade and P. B. Clarke, *J. Pharmacol. Exp. Ther.*, 2006, **317**, 1178–1187.
22 M. Perry, Q. Li and R. T. Kennedy, *Anal. Chim. Acta*, 2009, **653**, 1–22.
23 D. L. Robinson, A. Hermans, A. T. Seipel and R. M. Wightman, *Chem. Rev.*, 2008, **108**, 2554–2584.
24 B. J. Venton, H. Zhang, P. A. Garris, P. E. Phillips, D. Sulzer and R. M. Wightman, *J. Neurochem.*, 2003, **87**, 1284–1295.
25 A. L. Sanford, S. W. Morton, K. L. Whitehouse, H. M. Oara, L. Z. Lugo-Morales, J. G. Roberts and L. A. Sombers, *Anal. Chem.*, 2010, **82**, 5205–5210.
26 L. A. Gunaydin, O. Yizhar, A. Berndt, V. S. Sohal, K. Deisseroth and P. Hegemann, *Nat. Neurosci.*, 2010, **13**, 387–392.
27 V. Gradinaru, M. Mogri, K. R. Thompson, J. M. Henderson and K. Deisseroth, *Science*, 2009, **324**, 354–359.
28 V. S. Sohal, F. Zhang, O. Yizhar and K. Deisseroth, *Nature*, 2009, **459**, 698–702.
29 C. E. Bass, V. P. Grinevich, Z. B. Vance, R. P. Sullivan, K. D. Bonin and E. A. Budygin, *J. Neurochem.*, 2010, **114**, 1344–1352.
30 J. P. Britt, R. A. McDevitt and A. Bonci, *Curr. Protoc. Neurosci.*, 2012, **58**, 2.16.1–2.16.19.
31 C. N. Cearley and J. H. Wolfe, *Mol. Ther.*, 2006, **13**, 528–537.
32 U. Ungerstedt, *Acta Phys. Scand.*, 1971, **367**, 1–48.
33 C. A. Johnston, L. A. Mattiace and A. Negro-Vilar, *Cell. Mol. Neurobiol.*, 1987, **7**, 403–411.
34 J. Park, P. Takmakov and R. M. Wightman, *J. Neurochem.*, 2011, **119**, 932–944.
35 J. Park, B. M. Kile and R. M. Wightman, *Eur. J. Neurosci.*, 2009, **30**, 2121–2133.
36 J. Park, B. J. Aragona, B. M. Kile, R. M. Carelli and R. M. Wightman, *Neuroscience*, 2010, **169**, 132–142.
37 X. Xiao, J. Li and R. J. Samulski, *J. Virol.*, 1998, **72**, 2224–2232.
38 G. P. Gao, M. R. Alvira, L. Wang, R. Calcedo, J. Johnston and J. M. Wilson, *Proc. Natl. Acad. Sci. U. S. A.*, 2002, **99**, 11854–11859.
39 G. Paxinos and C. Watson, *The rat brain in stereotaxic coordinates*, Academic Press/Elsevier, Amsterdam, Boston, 2007.
40 P. S. Cahill and R. M. Wightman, *Anal. Chem.*, 1995, **67**, 2599–2605.
41 D. Michael, E. R. Travis and R. M. Wightman, *Anal. Chem.*, 1998, **70**, 586A–592A.
42 C. D. Kilts and C. M. Anderson, *Neurochem. Int.*, 1986, **9**, 437–445.
43 C. D. Kilts and C. M. Anderson, *Brain Res.*, 1987, **416**, 402–408.
44 B. J. Ciliax, C. Heilman, L. L. Demchyshyn, Z. B. Pristupa, E. Ince, S. M. Hersch, H. B. Niznik and A. I. Levey, *J. Neurosci.*, 1995, **15**, 1714–1723.
45 M. Rickhag, F. H. Hansen, G. Sorensen, K. N. Strandfelt, B. Andresen, K. Gotfryd, K. L. Madsen, I. Vestergaard-Klewe, I. Ammendrup-Johnsen, J. Eriksen, A. H. Newman, E. M. Fuchtbauer, J. Gomeza, D. P. Woldbye, G. Wortwein and U. Gether, *Nat. Commun.*, 2013, **4**, 1580.
46 K. K. Yung, J. P. Bolam, A. D. Smith, S. M. Hersch, B. J. Ciliax and A. I. Levey, *Neuroscience*, 1995, **65**, 709–730.
47 B. P. Bergstrom and P. A. Garris, *J. Neurochem.*, 2003, **87**, 1224–1236.
48 P. A. Garris and R. M. Wightman, *J. Neurosci.*, 1994, **14**, 442–450.
49 P. A. Garris, Q. D. Walker and R. M. Wightman, *Brain Res.*, 1997, **753**, 225–234.
50 O. P. Ernst, P. A. Sanchez Murcia, P. Daldrop, S. P. Tsunoda, S. Kateriya and P. Hegemann, *J. Biol. Chem.*, 2008, **283**, 1637–1643.
51 Z. F. Mainen, J. Joerges, J. R. Huguenard and T. J. Sejnowski, *Neuron*, 1995, **15**, 1427–1439.
52 C. E. Bass, V. P. Grinevich, D. Gioia, J. D. Day-Brown, K. D. Bonin, G. D. Stuber, J. L. Weiner and E. A. Budygin, *Front. Behav. Neurosci.*, 2013, **7**, 173.
53 Q. Wu, M. E. Reith, Q. D. Walker, C. M. Kuhn, F. I. Carroll and P. A. Garris, *J. Neurosci.*, 2002, **22**, 6272–6281.
54 J. A. Javitch, S. M. Strittmatter and S. H. Snyder, *J. Neurosci.*, 1985, **5**, 1513–1521.
55 D. Sulzer, N. T. Maidment and S. Rayport, *J. Neurochem.*, 1993, **60**, 527–535.
56 E. S. Ramsson, D. P. Covey, D. P. Daberkow, M. T. Litherland, S. A. Juliano and P. A. Garris, *J. Neurochem.*, 2011, **117**, 937–948.
57 M. C. Ritz, R. J. Lamb, S. R. Goldberg and M. J. Kuhar, *Science*, 1987, **237**, 1219–1223.
58 R. M. Wightman, M. L. Heien, K. M. Wassum, L. A. Sombers, B. J. Aragona, A. S. Khan, J. L. Ariansen, J. F. Cheer, P. E. Phillips and R. M. Carelli, *Eur. J. Neurosci.*, 2007, **26**, 2046–2054.
59 L. A. Sombers, M. Beyene, R. M. Carelli and R. M. Wightman, *J. Neurosci.*, 2009, **29**, 1735–1742.
60 B. J. Venton and R. M. Wightman, *Synapse*, 2007, **61**, 37–39.
61 W. X. Shi, C. L. Pun and Y. Zhou, *Neuropsychopharmacology*, 2004, **29**, 2160–2167.
62 N. D. Volkow, D. Tomasi, G. J. Wang, J. Logan, D. L. Alexoff, M. Jayne, J. S. Fowler, C. Wong, P. Yin and C. Du, *Mol. Psychiatry*, 2014, **19**, 1037–1043.
63 N. D. Volkow, G. J. Wang, J. S. Fowler, J. Logan, S. J. Gately, R. Hitzemann, A. D. Chen, S. L. Dewey and N. Pappas, *Nature*, 1997, **386**, 830–833.